RESEARCH PAPER

Facile fabrication, characterization and enhanced heterogeneous catalytic reduction of 4-nitrophenol using undoped and doped ZrO_2 nanoparticles

Guguloth Ravi [1], Dasari Ayodhya [1], Madderla Sarasija [2], Dongamanti Ashok [1,*]

[1] *Department of Chemistry, Osmania University, Hyderabad-500007, Telangana State, India*

[2] *Department of Chemistry, Satavahana University, Karimnagar-505002, Telangana State, India*

ARTICLE INFO

Article History:
Received 11 December 2018
Accepted 14 March 2019
Published 15 June 2019

Keywords:
ZrO_2 NPs
Co-precipitation Method
Dopants
4-Nitrophenol Reduction
Kinetics

ABSTRACT

Here, we successfully developed the undoped, Ni^{2+}, Cu^{2+}, and Zn^{2+} doped Zirconia nanoparticles (ZrO_2 NPs) by a simple co-precipitation method at room temperature. The synthesized materials were characterized by various physicochemical measurement techniques to investigate their structure, morphology, and size of the particles. The bandgap energy values of doped and undoped ZrO_2 NPs were estimated using optical absorption spectroscopy, which were found to be in the range of 4.1-4.4 eV. The UV (304-352 nm) and visible (402-415 nm) emissions and the oxygen vacancies and band gap of the particles were investigated through PL analysis. The structure, morphology, and well-dispersed particles with the size in the range of 10-40 nm of the prepared ZrO_2 NPs were deliberated by SEM and TEM analyses. The Zr–O stretching vibration and Zr–O–Zr bending vibrations were confirmed through FTIR analysis. The catalytic reduction of 4-nitrophenol (4-NP) using $NaBH_4$ as a reducing agent was studied by the prepared doped and undoped ZrO_2 NPs. The efficient catalytic activity was observed in the presence of Cu^{2+} doped ZrO_2 NPs than the Zn^{2+}, Ni^{2+} doped and undoped ZrO_2 NPs due to the small size and large surface area of the particles. The results showed 97% conversion of 4-NP to 4-aminophenol (4-AP) within 90 min, and a stability up to 5 consecutive recycles.

How to cite this article
Ravi G, Ayodhya D, Sarasija M, Ashok D. Facile fabrication, characterization and enhanced heterogeneous catalytic reduction of 4-nitrophenol using undoped and doped ZrO_2 nanoparticles. Nanochem Res, 2019; 4(1):43-54. DOI: 10.22036/ncr.2019.01.006

INTRODUCTION

In recent times, the urgent need to develop clean and green chemical process is inevitable in order to circumvent the environmental concerns [1]. Due to the continuous increase in industrialization, the release of hazardous pollutants generates bad impact on environment and human being. Among these hazardous pollutants, aromatic nitro compounds are life-threatening substances due to their noxious and mutagenic nature [1]. Aromatic nitro compounds are the main organic effluents from the wastewater of industries and agricultural waste. Generally, waste water contains p-nitrophenol (4-NP), which is highly toxic and carcinogenic in nature and also causes harmful effect on the ecosystem. Introduction of 4-NP in the human body decreases oxygen storage capacity of blood, causing methaemoglobinaemia and several other chronic diseases [2-3]. In contrast, 4-AP is an important feedstock for the synthesis of various analgesic and antipyretic drugs in pharmaceuticals. Para-aminophenol obtained from 4-NP reduction is an important intermediate for the synthesis of paracetamol and also other much more valuable chemicals for the synthesis of dyestuffs, photographic chemicals, polymer,

* Corresponding Author Email: *ashokdou@gmail.com*

surfactant, corrosion inhibitor and anti-corrosion lubricant [4-6].

Metal and metal oxide nanoparticles bear unique, intriguing, and versatile electronic, optical, and catalytic properties. They have been extensively studied by researchers in the field of chemical catalysis, organic synthesis, and electro-analytical reaction since last few decades [7-10]. Much research has been focused on the catalytic reduction of organic molecules, based on the high chemical activity for the chemolysis of environmental pollutants [11]. More exclusively, the application of metal and metal oxide nanoparticles as catalysts to reduce nitro compounds into amines is acknowledged universally due to their proficient catalytic activity in aqueous media. For example, Wang et al. have demonstrated that Au nanoparticles decorated on N-containing polymer spheres are highly active in the reduction of 4-nitrophenol (4-NP) to 4-aminophenol (4-AP) [12]. Feng et al. fabricated the Pt-Au dendrite with a highly branched nanostructure supported on the graphene oxide and studied their catalytic activity [13]. Chen et al. reported that the synergistic interaction between Au and Pd nanoparticles in a nanosheet graphene support the facilitated reduction of 4-NP [14]. However, widespread applications of such noble metal catalysts are severely limited due to their high costs. In the interim, low cost, relatively high abundance, and nontoxic nature of ZrO_2-based nanoparticles make them potential alternatives to the various metals for the catalytic applications. Recently, ZrO_2 based composites have been successfully synthesized and utilized for the efficient reduction of 4-NP [15-16].

Wide bandgap semiconductors like ZnO, Ag_2S, TiO_2, ZnS, SiO_2, CdS, Bi_2S_3, and ZrO_2 are well-suited catalysts for the abatement of water pollution [15-23]. Among these wide band gap semiconductors, the metallic ZrO_2 nanoparticles have been received significant attention because of their various potential applications [24], and also play a significant role in catalysis research because of their high surface to volume ratio [25]. ZrO_2 is an n-type semiconductor with a bandgap of ~5 eV showing a very good catalytic performance under UV light irradiation [25]. At atmospheric pressure, ZrO_2 has three different types of crystalline structures: monoclinic (< 1170°C), tetragonal (between 1170 °C to 2370 °C) and cubic (> 2370 °C). Moreover, it has different infrared frequencies for cubic (480 cm^{-1}), tetragonal (435 cm^{-1}) and monoclinic (270 cm^{-1}) structures. This indicates that the optical phonon energy of ZrO_2 depends on the crystalline structures [25]. Generally, the applications of ZrO_2 nanoparticles strongly depend on the crystalline structure and the phase transformations. Furthermore, there are different techniques to synthesize ZrO_2 NPs [26-32]. Duran et al. also reported the synthesis of m-ZrO_2 nanopowder using a ball-milling-assisted hydrothermal technique [32]. Taguchi et al. prepared single phase, m-ZrO_2 nanocrystals under subcritical hydrothermal conditions [33]. Lee et al reported the microstructure of Y_2O_3-doped ZrO_2-CeO_2 composite NPs with a tetragonal crystalline phase [27]. However, it is a non-toxic, eco-friendly material, with greater thermal and chemical stability, and cost-effectiveness.

Herein, we have synthesized Cu^{2+}, Ni^{2+}, Zn^{2+} doped and undoped ZrO_2 NPs through a simple, fast, high yielding and easy to purify the particles using the co-precipitation method. The synthesized ZrO_2 NPs were characterized using UV-Vis DRS, FTIR, XRD, PL, SEM, and TEM techniques. The effect of undoped and doped ZrO_2 NPs in the catalytic reduction of 4-NP to 4-AP has been investigated in detail. It was found that the presence of dopants significantly improves the catalytic performance of ZrO_2 in the 4-NP reduction than the undoped ZrO_2 NPs due to the doping effect of metal ions leading to an increase in number of active sites on the surface area. The present study may utilize in the removal of aqueous pollutants in a cleaning of environmental pollution as well as in industrial applications.

EXPERIMENTS

Materials and Methods

All the materials were obtained from commercial suppliers and used without further purification. The double distilled water used as a solvent for the preparation of stock solutions. The precursors used for the synthesis of doped and undoped ZrO_2 NPs were Zirconyl chloride octahydrate ($ZrOCl_2 \cdot 8H_2O$) purchased from Sigma-Aldrich and ammonium hydroxide solution (NH_4OH), nickel acetate, copper acetate, and zinc acetate were purchased from Merck chemical, India.

Synthesis of undoped ZrO_2 nanoparticles

In a typical synthesis, 0.05 M of Zirconyl chloride octahydrate was dissolved in 100 ml of double distilled water, to which the NH_4OH

solution was slowly added, and stirred rapidly while maintaining a pH of 10. The above-prepared solution was moved into a reaction vessel which is present on the magnetic stirrer at 5000 rpm speed and 2 hours for the continue stirring at 60 °C after which it was allowed to cool down to room temperature. The product was centrifuged, washed with distilled water and acetone several times, dried at 90°C and calcined at 450 °C for 60 min. Finally, the obtained ZrO_2 NPs were subjected to a number of physicochemical characterization techniques.

Synthesis of Ni^{2+}, Cu^{2+} and Zn^{2+} doped ZrO_2 nanoparticles

In a typical synthesis, 0.05 M of Zirconyl chloride octahydrate and 0.01 M metal salts solution (nickel acetate for Ni^{2+} doping; copper acetate for Cu^{2+} doping; and zinc acetate for Zn^{2+} doping) were dissolved in 100 ml of double distilled water to which the NH_4OH solution was slowly added, and was stirred rapidly while maintaining at a pH of 7-11. The above-prepared solution was moved into a reaction vessel which is present on the magnetic stirrer at 5000 rpm speed and 2 h for the continuous stirring at 60 °C after which it was allowed to cool down to room temperature. The product was centrifuged, washed with distilled water and acetone several times, dried at 90 °C and calcined at 450 °C for 60 min. Finally, the obtained Ni^{2+}, Cu^{2+} and Zn^{2+} doped ZrO_2 NPs were subjected to a number of physicochemical characterization techniques.

Characterizations

The morphology of the doped and undoped ZrO_2 NPs was characterized by scanning electron microscopy (SEM, ZEISS EVO18, 15 kV) with energy-dispersive X-ray spectroscopy (EDX). The crystal structure of the prepared ZrO_2 NPs was investigated with transmission electron microscopy (TEM, TECHNAI G2) operated at 100 kV and X-ray diffraction (XRD, Xpert Philips, Bruker X-ray diffractometer equipped with graphite-monochromated CuKα radiation at λ = 1.541 A°) with a 2θ range of 10-80°. UV-Vis-NIR spectrophotometer (Shimadzu UV-3600) was used to record the UV-Vis diffuse reflectance spectra (UV-Vis DRS) to measure the absorbance characteristics of ZrO_2, and $BaSO_4$ was used as a reference standard to examine the optical properties of the samples in the wavelength range of 200-800 nm. Room temperature photoluminescence (PL) properties of the products were studied on a Perkin-Elmer (5301-PC) fluorescence spectrophotometer. The FTIR spectra were recorded in transmittance mode on a Shimadzu spectrophotometer in the wave number range of 400-4000 cm^{-1}.

Catalytic reduction of 4-nitrophenol

The catalytic reduction of 4-NP to 4-AP was employed as a model reaction to evaluate the catalytic performance of the undoped and Ni^{2+}, Cu^{2+} and Zn^{2+} doped ZrO_2 NPs. At the beginning, 15 mL of 1.5×10^{-4} M 4-NP aqueous solution was added into 5 mL of freshly prepared 0.05 M $NaBH_4$ solution, resulting in a dark yellow solution. Then, a homogeneously dispersed aqueous solution containing 1 mg of doped and undoped ZrO_2 catalyst was added to the mixed solution at room temperature separately. The reaction was monitored by immediately taking a small portion of the solution that was put into a quartz cuvette for the UV-Vis absorption measurements in the range of 200–550 nm by a UV-Vis double beam spectrophotometer (UV-3600 series double beam spectrophotometer, Shimadzu). The slope of the plot of relative intensity of the absorbance ln (A_0/A_t) at 400 nm versus time gives the rate constant (k).

Reusability of the catalyst

A series of catalytic experiments were performed for the reusability and stability of the catalyst as doped and undoped ZrO_2 NPs. After each cycle of catalytic reaction, the synthesized ZrO_2 NPs were separated and collected by centrifugation. Afterward, the sample was washed with 50 mL distilled water several times, and vacuum dried at 70°C. The same procedure was repeated for each recycle test.

RESULTS AND DISCUSSION

UV-Vis absorption analysis

The UV-Vis absorption spectra of the synthesized undoped and doped ZrO_2 NPs are shown in Fig. 1. It represents the optical absorption spectrum of ZrO_2 NPs showing a sharp optical absorption band at 280 nm due to the transition from the valence band to the conduction band, and still, there is some support from the extrinsic states to the absorption in the UV region [34]. Along with this peak, a weak absorption peak is also identified at 230 nm. The observed absorption band may be due to the charge transfer transition ($O^{2-}\rightarrow Zr^{4+}$)

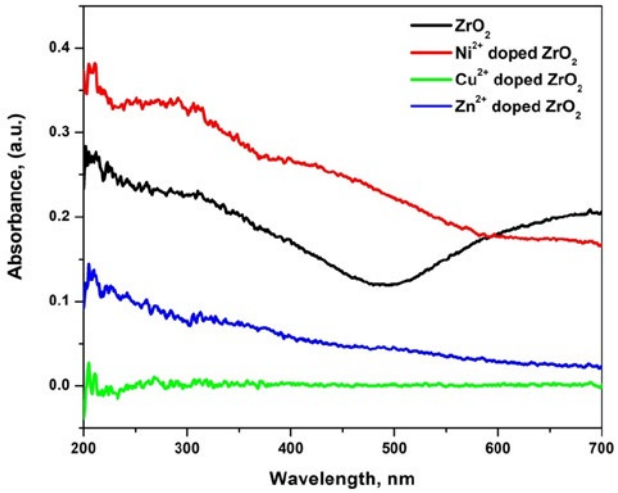

Fig. 1. The room temperature optical absorption spectrum of undoped and doped ZrO_2 NPs.

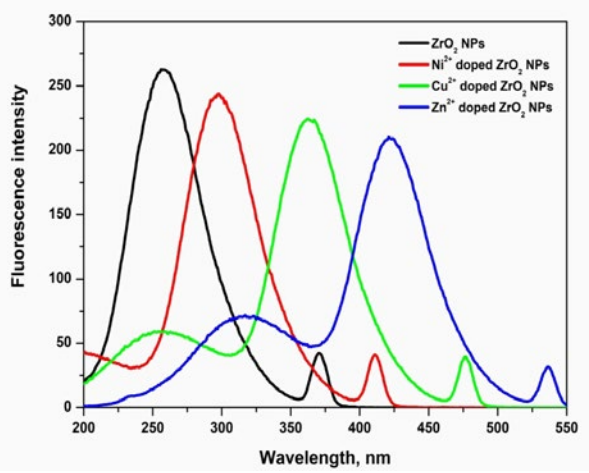

Fig. 2. The room temperature PL spectrum of undoped and doped ZrO_2 NPs.

corresponding to the excitation of the electron from valence band to conduction band. This transition takes place from 2p energy state of O to 4d (x_2-y_2, z_2) energy state of Zr, since the valence band of ZrO_2 is mainly composed of the occupied 2p energy state of the oxygen atom and the conduction band is constituted by unoccupied energy state 4d (x_2-y_2,z_2) of Zr atom. Moreover, no characteristic peak of d-d transition is observed in the visible region since the Zr^{4+} ions have d^0 configuration. However, the observed absorption peak in the UV-range is at a lesser energy compared to the literature on the optical band gap for bulk ZrO_2 [35]. The size reduction in the NPs can cause the change in the optical band gap of metal oxides over the narrowing of the valence and conduction bands. The obtained direct band gap value of doped and undoped ZrO_2 nanoparticles is found to be 4.14 to 4.46 eV. The obtained value is in a good agreement with values reported in the literature [34-35].

Photoluminescence analysis

Photoluminescence technique is a suitable method to determine the crystalline quality, presence of impurities as well as exciton (bound state of an electron and an electron hole) fine structure. Moreover, it can also be used to study the migration, transfer and recombination rate of photogenerated electron-hole pairs in the semiconductor. In general, pure ZrO_2 shows the different broadband emissions, which are dependent on the preparation methods and excitation wavelength [36]. Fig. 2

shows the PL spectrum of ZrO_2 NPs excited at 350 nm, it exhibits three emission bands at 372, 412 and 535 nm. Owing to the non-luminous nature of Zr^{4+}, the observed emission peaks can be attributed to its non-stoichiometry resulting from the oxygen deficiency in the ZrO_2 system. The peak observed at 372 nm corresponds to the ionized oxygen vacancies from the conduction band to the valence band. The broad emission band observed at 412 nm is ascribed to the Zr vacancy and is one of the most intense bands to consider the band edge emission due to the free-exciton recombination [37]. Due to the influence of surface defects and oxygen vacancies a peak is observed at 537 nm. This green emission band (535 nm) indicates the surface defects in the ZrO_2 lattice [38]. The similar results have been reported in the literature for ZrO_2 systems [39].

FTIR analysis

FTIR spectroscopic measurements were carried out to identify the interactions between the dopants on the surface of the ZrO_2 NPs which are specifically involved in the formation of nanoparticles. The existence of functional groups in the synthesized samples is examined using the FT-IR technique in the range of 400 to 4000 cm^{-1} and are shown in Fig. 3. From the spectrum, peaks observed at 480 and 580 cm^{-1} are due to the Zr–O vibration mode confirming the formation of ZrO_2 structure [40]. A band identified at 741 cm^{-1} is corresponding to metal-Zr bond in doped ZrO_2 NPs. The bands observed at 1631 and 3426 cm^{-1} correspond to the vibration mode from the moisture absorbed on the samples and stretching vibrations of the O-H bond and indicates the existence of hydroxyl groups on the surface of the sample. Fig. 3 depicts a broad prominent band around 3200-3400 cm^{-1} related to the –OH stretching vibrations of adsorbed water molecules on the prepared sample. It is well known that the peaks at 705 and 634 cm^{-1} are distinctive for Zr–O–Zr vibrations. The existence of Zr–OH vibrations can be evidenced by the appearance of a peak at 530 cm^{-1}. It is apparent that the intensity of absorption in the region of 500-700 cm^{-1} characteristic of tetragonal Zr–O–Zr vibrations is greatly enhanced by calcination at 500°C. Moreover, the peak characteristic of Zr–OH vibration disappeared due to the condensation of hydroxyl groups to form ZrO_2.

XRD analysis

To confirm the phase formation of undoped and doped ZrO_2 NPs using powder X-ray diffraction (XRD) is recorded in an air atmosphere (Fig. 4). All of the dominant diffraction peaks in the XRD pattern can be identified as the tetragonal ZrO_2 phase with indices of (1 1 1), (2 0 0), (2 2 0), (3 1 1), and (2 2 2) crystalline planes, respectively (JCPDS Card No. 02-0733) [41]. There are no peaks of other phases (especially, monoclinic phase) observed in the XRD pattern. This clarifies that the synthesized ZrO_2 NPs contain a single crystalline tetragonal phase without any phase impurities. It can also be clearly observed that the synthesized ZrO_2 NPs exhibit high crystallinity due to the intensity sharpness of all the dominant diffraction peaks. Using the Debye-Scherrer formula, the average

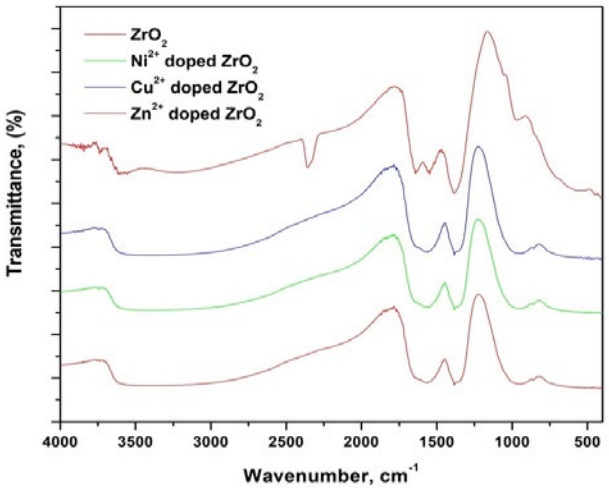

Fig. 3. FTIR spectra of the doped and undoped ZrO_2 NPs.

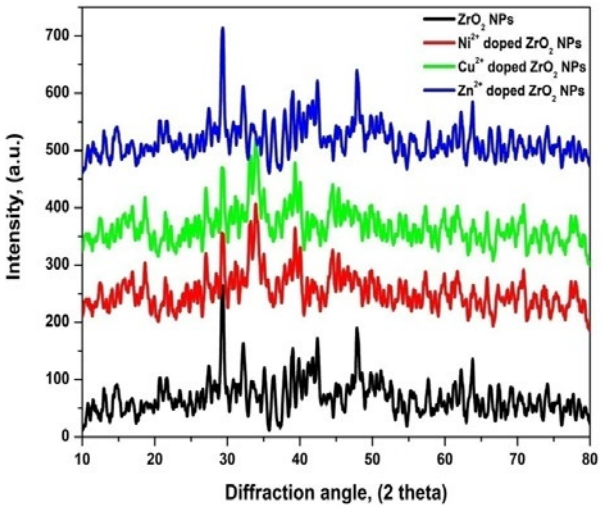

Fig. 4. X-ray diffraction patterns for undoped and doped ZrO_2 NPs.

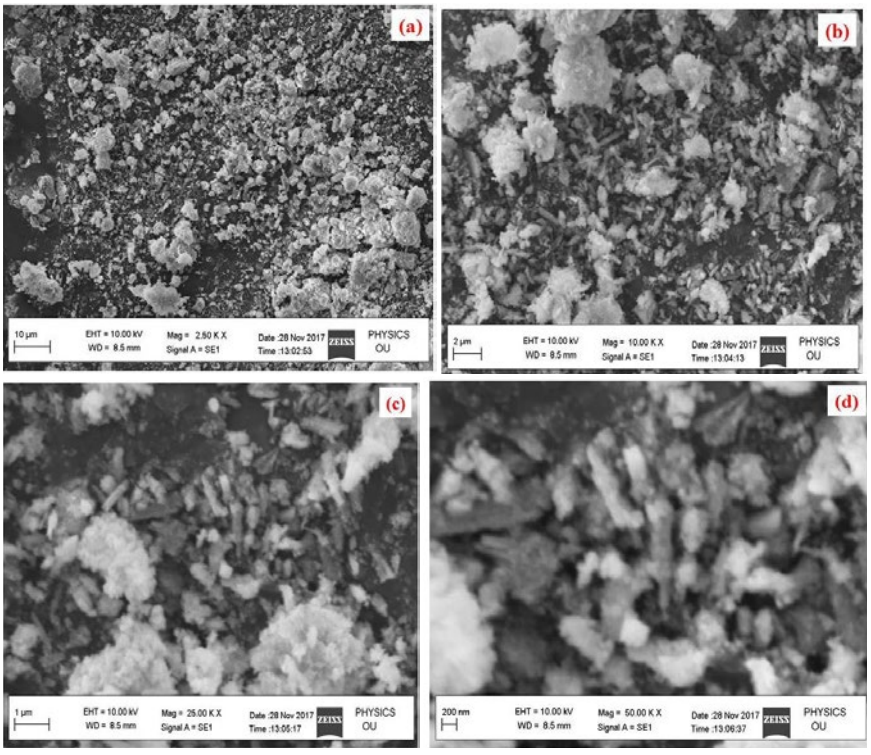

Fig. 5. (a-d) SEM images of ZrO_2 nanoparticles with different magnifications.

crystallite size of undoped and Cu^{2+}, Ni^{2+}, Zn^{2+} doped ZrO_2 NPs was found to be 24±0.5 nm, 13±0.8 nm, 17±0.6 nm and 15±0.2 nm, respectively.

SEM analysis

Fig. 5(a-d) shows the surface morphology of the prepared undoped and doped ZrO_2 NPs examined by SEM analysis at different magnifications. It is clear from Fig. 5 that the ZrO_2 NPs are in uniform size indicating that the ZrO_2 particles are spherical in nature with nanometer region. The agglomeration of some small and uniform-sized

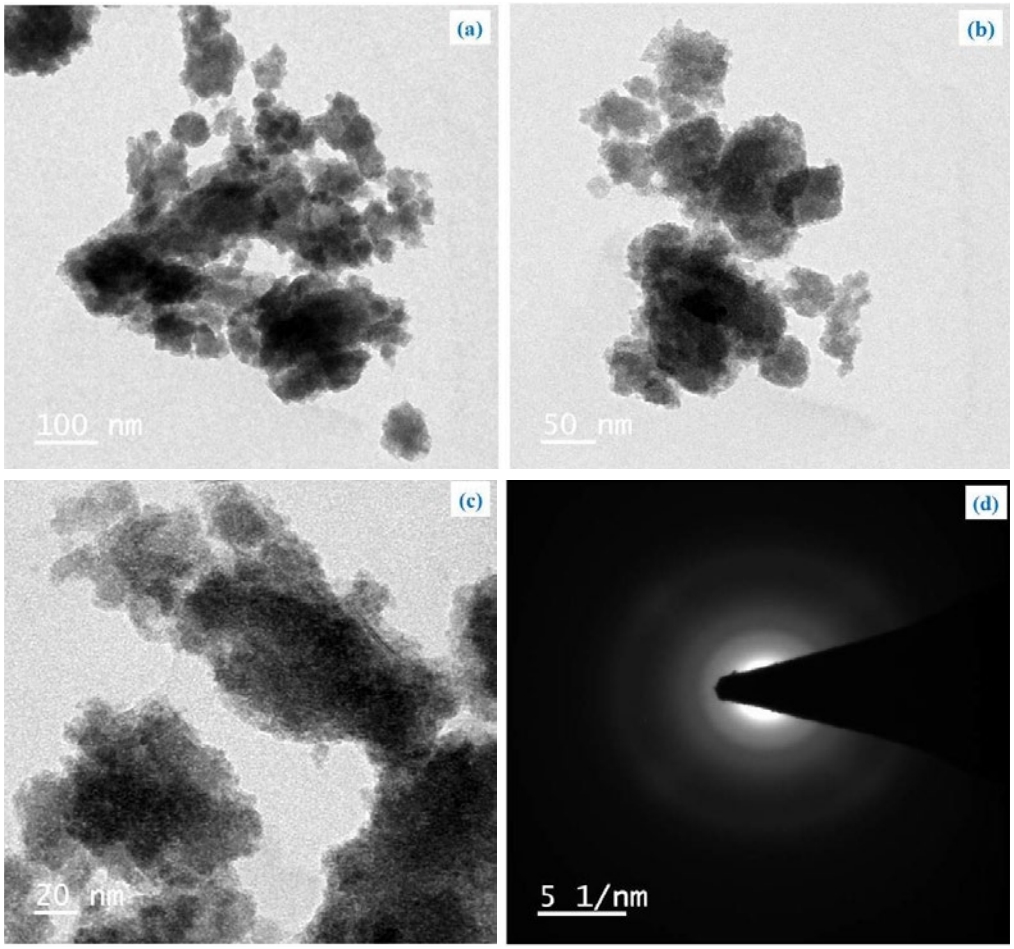

Fig. 6. (a-c) TEM images of ZrO_2 NPs with different magnifications and (d) SAED pattern.

ZrO_2 NPs as a cluster was initially observed. The calculated crystallite size was in the range of less than 50 nm for different samples of ZrO_2 NPs. It is observed that most of the particles are spherical in shape with smooth and fused surface. The energy dispersive X-ray (EDX) spectra of undoped ZrO_2 NPs show only the presence of Zr and O atoms, indicating the absence of impurities from the sintered samples.

TEM analysis

To get further evidence on structural information of the synthesized ZrO_2 NPs, TEM and selected area electron diffraction (SAED) analyses were carried out. Fig. 6(a-c) shows the TEM images of ZrO_2 NPs at different magnifications and it is clear that the NPs are spherical in shape and uniform in size. The TEM image of ZrO_2 NPs shown in Fig. 6 indicates the existence of well-organized particles and small agglomerated particles of ZrO_2. The fringe arrangements inside the crystallite show the development of a single phase ZrO_2 with an extended order in the crystalline structure. The corresponding SAED pattern of the synthesized ZrO_2 NPs is shown in Fig. 6(d). The obtained average crystallite size from TEM is 10-25 nm; it is slightly higher than the value obtained by XRD. This difference between the XRD and TEM results may be due to the aggregation of the small particles of ZrO_2.

Catalytic reduction of 4-nitrophenol

To study the catalytic performance of the as-prepared catalysts (undoped and doped ZrO_2 NPs), a model catalytic reaction involving the reduction of 4-NP by excess $NaBH_4$ was carried out, and the UV-Vis spectrometry was used to monitor the entire reaction process, as depicted in Fig. 7. After adding a certain amount of $NaBH_4$ solution into 4-NP solution, the absorption peak exhibited an

obvious blue shift from 319 nm to 400 nm (Fig. 7), mainly due to the formation of 4-nitrophenolate ions in alkaline environments [42]. The intensity of the absorption peak at 400 nm could remain nearly unchanged with time in the presence of $NaBH_4$ [43]. Fig. 7 shows the UV-Vis absorption spectra of the reactant 4-NP solution over time in the presence of $NaBH_4$ and the absence and presence of ZrO_2 NPs. As we can see, the absorption intensity remained almost the same over time indicating no catalytic property without catalyst. With addition of ZrO_2 NPs as a catalyst into the reaction mixture, the characteristic absorption peak at 400 nm gradually decreased in intensity along with the fading of the yellow-green color. Meanwhile, a new absorption peak at about 300 nm (assigned to 4-AP) appeared and increased gradually over time suggesting that the chemical reaction happened in the presence of the synthesized ZrO_2 catalysts.

The conversion of 4-NP to 4-AP was monitored by recording the intensity changes of the absorbance bands of the reactant 4-NP and the product 4-AP centered at 400 and 303 nm, respectively. The reaction remained almost unchanged without the addition of catalyst due to the high kinetic barrier between the mutually repelling negative ions: 4-NP and BH^{4-}. The color of the 4-NP solution changed from light yellow to yellow-green after the addition of $NaBH_4$. Consequently, the alkali mediated formation of phenolate ion (317 nm), which

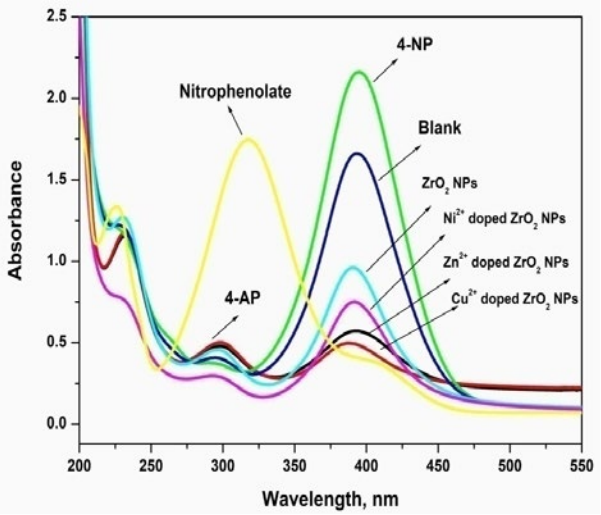

Fig. 7. The UV-Vis spectra of 4-NP reduction with undoped and doped ZrO_2 NPs.

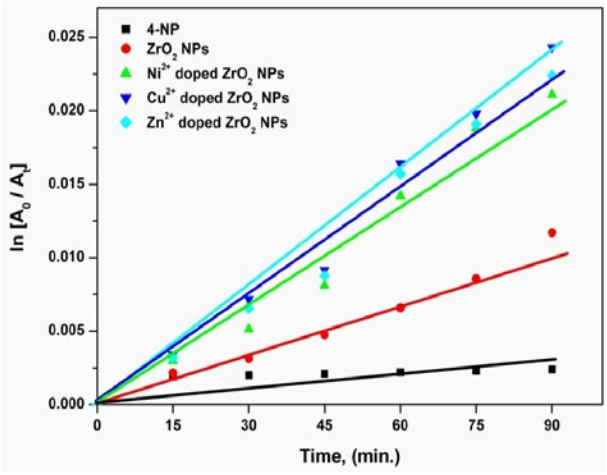

Fig. 8. Linear plots of $\ln(A_0/A_t)$ vs. time for the catalytic reduction of 4-nitrophenol over the synthesized undoped and doped ZrO_2 NPs.

resulted in the shifting of a strong absorption peak of 4-NP at 400 nm, as shown in Fig. 7. However, the absorbance peak at 400 nm remained unaffected in the case of the undoped ZrO_2 NPs, as shown in Fig. 7. The time-dependent UV-Vis spectra for undoped ZrO_2 NPs serving as the catalyst showed the rapid decrease in the intensity of the absorbance peak of the 4-NP ion at 400 nm, with the simultaneous increase in the intensity of the 4-AP absorbance peak at 303 nm (Fig. 7) suggesting the conversion of 4-NP to 4-AP using $NaBH_4$. With addition of undoped ZrO_2 NPs (1 mg), the yellow color of the 4-NP solution was completely bleached within 45 min (Fig. 7), suggesting that the reaction was rapidly completed.

However, the complete conversion of 4-NP to 4-AP was achieved within 90 min by the Ni^{2+}, Cu^{2+} and Zn^{2+} doped ZrO_2 NPs samples, respectively, as shown in Fig. 7. From the time-dependent UV–Vis absorbance spectra, the catalytic activities are in the following order: Zn^{2+} doped ZrO_2 NPs > Ni^{2+} doped ZrO_2 NPs > Cu^{2+} doped ZrO_2 NPs. It can be inferred that the important aspect of the catalytic reduction of 4-NP involves the enhanced diffusion and adsorption of 4-NP to the catalytic surface and consequential electron transfer mediated by the catalytic surface from BH^{4-} to 4-NP as suggested by previous report [44]. The particle size of these catalysts also has great influence on their catalytic activities. For instance, the catalytic activity was observed by varying the particle sizes of doped (Ni^{2+}, Cu^{2+} and Zn^{2+}) ZrO_2 NPs and it was measured by TEM analysis. These catalytic reaction times were quite longer than the time required for smaller sized particles (around 12 nm) of Zn^{2+} doped ZrO_2 NPs. This suggested that smaller nanoparticles were more catalytically active than the larger size particles of doped ZrO_2 NPs than the undoped ZrO_2 NPs due to the large surface area of smaller particles which led to enhance diffusion and rapid adsorption.

The conversion percentage (α) of 4-NP to 4-AP was calculated by the formula:

$$\alpha = A_0 / A_t \times 100\%$$

It was found that the reduction of 4-NP to 4-AP by sodium borohydride in the presence of ZrO_2 NPs as catalyst follows pseudo-first order rate equation with respect to 4-NP because the concentration of $NaBH_4$ was too high as compared to 4-NP. So, the concentration of $NaBH_4$ was considered constant throughout the reaction.

Evaluation of rate constants

In the catalytic reduction reaction, the concentration of $NaBH_4$ was very high and could be considered as a constant during the reaction period. Hence, pseudo-first-order kinetics could be applied to evaluate the catalytic activity of the catalysts [45]. The plot of ln (A_0/A_t) versus time is obtained based on the absorbance as a function of time. The good linear correlations observed, as shown in Fig. 8, signify that the reactions follow the first-order kinetics. The ratios of A_0 to A_t were obtained from the relative intensity ratios

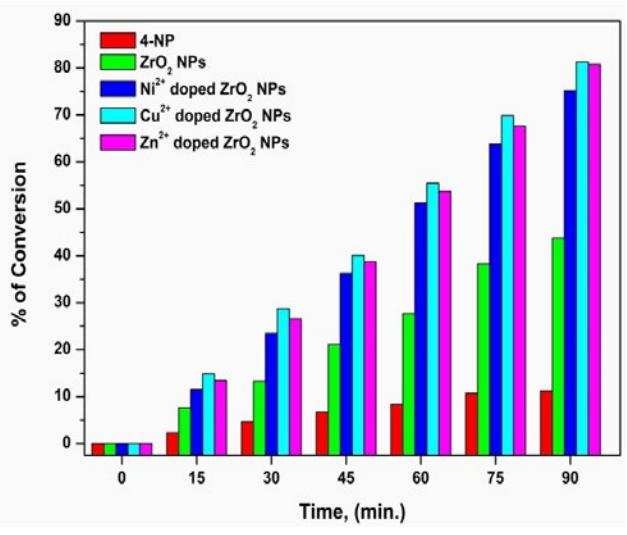

Fig. 9. The catalytic conversion of undoped and doped ZrO_2 NPs catalyst for the reduction of 4-NP with $NaBH_4$.

of the respective absorbance (A_o/A_t) at 400 nm, in which t is the reaction time, and A_0 and A_t are the absorbances of 4-NP at the time 0 and t, respectively. The rate constant k can be determined by the rate equation ln (A_0/A_t) = -kt. The reaction rate constant k was determined from the slope of the plots of ln (A_0/A_t) vs. time as shown in Fig. 8. The reaction rate constant k was found to be 2.21 × 10^{-2} s^{-1} for undoped ZrO_2 NPs, 2.49 × 10^{-2} s^{-1} for Cu^{2+} doped ZrO_2 NPs, 3.25× 10^{-2} s^{-1} for Ni^{2+} doped ZrO_2 NPs and 5.8 × 10^{-3} s^{-1} for Zn^{2+} doped ZrO_2 NPs. It was observed that the Zn^{2+} doped ZrO_2 NPs sample exhibits the best catalytic activity among the other doped and undoped ZrO_2 NPs. The catalytic conversion of 4-NP clearly indicates the maximum catalytic activity in the presence of Cu^{2+} doped ZrO_2 NPs comparing to the undoped and Ni^{2+}, Zn^{2+} doped ZrO_2 NPs, as shown in Fig. 9.

Reusability of the synthesized undoped and doped ZrO_2 NPs

The reusability of nanocatalysts is an important aspect to be strongly considered in practical heterogeneous catalytic applications. To evaluate the reusability of the synthesized ZrO_2 NPs as catalyst, repetitive reduction cycles were performed under similar conditions. The kinetic constant of the first run was taken as a control and the reaction conditions were kept constant for successive cycles. In addition, the activity ratio was defined as the ratio of the kinetic constant in each run to one of the first runs. It was explored up to five cycles and excellent reusability was demonstrated for the Cu^{2+} doped ZrO_2 NPs sample. It possesses superior reusability and regeneration, consistently maintaining approximately 94.5% reduction conversion of 4-NP in all five cycles with loss of slight activity. The slight decrease after the third cycle might be due to some loss of the nanocomposite catalyst during the recurrent sample washing.

CONCLUSION

In this study, we report the synthesis of undoped, Ni^{2+}, Cu^{2+} and Zn^{2+} doped ZrO_2 NPs using a simple co-precipitation method. The catalytic activities of the synthesized materials towards the reduction of 4-NP to 4-AP were comparatively investigated using $NaBH_4$ as a reducing agent. The morphology, structure and optical properties of the synthesized ZrO_2 NPs were characterized using TEM, SEM, XRD, FTIR, UV-Vis, and PL spectroscopy. The crystal structure and size of ZrO_2 NPs were confirmed by XRD and TEM. The well dispersed doped ZrO_2NPs having the size 10-25 nm was exhibited from the TEM analysis. Among the undoped and doped ZrO_2 NPs, Cu^{2+} doped ZrO_2 NPs are the superior catalysts for the reduction of 4-NP to 4-AP due to the small size of the particles and large surface area. The Zr_2O NPs, bearing high surface area along with the formation of highly active with dopants (Ni^{2+}, Cu^{2+} and Zn^{2+}) during catalysis, trigger fast 4-NP reduction with an exceptionally high rate constant. In addition, the doped ZrO_2 NPs possessed remarkable reusability up to 5 consecutive cycles under similar conditions. Our results demonstrate that the synthesized ZrO_2 NPs can be a promising material of choice for various practical applications in catalysis and environmental applications.

ACKNOWLEDGMENTS

The authors (Dr. Guguloth Ravi) gratefully acknowledge to UGC, New Delhi, India for Post-Doctoral Fellowship. The authors would like to thank DST-FIST, New Delhi, India for providing necessary analytical facilities and express sincere thanks to the Head, Department of Chemistry, Osmania University for providing infrastructure and other necessary facilities.

CONFLICT OF INTEREST

The authors declared to no conflict of interest.

REFERENCES

[1] Ayodhya D, Veerabhadram G. A review on recent advances in photodegradation of dyes using doped and heterojunction based semiconductor metal sulfide nanostructures for environmental protection. Materials Today Energy. 2018;9:83-113.

[2] Ayodhya D, Veerabhadram G. Influence of g-C3N4 and g-C3N4 nanosheets supported CuS coupled system with effect of pH on the catalytic activity of 4-NP reduction using NaBH4. FlatChem. 2019;14:100088.

[3] Ibrahim I, Ali IO, Salama TM, Bahgat AA, Mohamed MM. Synthesis of magnetically recyclable spinel ferrite (MFe2O4, M=Zn, Co, Mn) nanocrystals engineered by sol gel-hydrothermal technology: High catalytic performances for nitroarenes reduction. Applied Catalysis B: Environmental. 2016;181:389-402.

[4] Kleist W, Pröckl SS, Drees M, Köhler K, Djakovitch L. Amination of aryl chlorides and fluorides toward the synthesis of aromatic amines by palladium-catalyzed route or transition metal free way: Scopes and limitations. Journal of Molecular Catalysis A: Chemical. 2009;303(1-2):15-22.

[5] Koutros S, Lynch CF, Ma X, Lee WJ, Hoppin JA, Christensen CH, et al. Heterocyclic aromatic amine pesticide use and human cancer risk: Results from the U.S. Agricultural Health Study. International Journal of Cancer. 2009;124(5):1206-12.

[6] Pacheco AdO, Kagohara E, Andrade LH, Comasseto JV, Crusius IHS, Paula CR, et al. Biotransformations of nitro-aromatic compounds to amines and acetamides by tuberous roots of Arracacia xanthorrhiza and Beta vulgaris and associated microorganism (Candida guilliermondii). Enzyme and Microbial Technology. 2007;42(1):65-9.
[7] Sravanthi K, Ayodhya D, Swamy PY. Green synthesis, characterization and catalytic activity of 4-nitrophenol reduction and formation of benzimidazoles using bentonite supported zero valent iron nanoparticles. Materials Science for Energy Technologies. 2019;2(2):298-307.
[8] Hughes MD, Xu Y-J, Jenkins P, McMorn P, Landon P, Enache DI, et al. Tunable gold catalysts for selective hydrocarbon oxidation under mild conditions. Nature. 2005;437(7062):1132-5.
[9] Ravi G, Sarasija M, Ayodhya D, Kumari LS, Ashok D. Facile synthesis, characterization and enhanced catalytic reduction of 4-nitrophenol using NaBH4 by undoped and Sm3+, Gd3+, Hf3+ doped La2O3 nanoparticles. Nano Convergence. 2019;6(1).
[10] Esquivel-Peña V, Bastos-Arrieta J, Muñoz M, Mora-Tamez L, Munguía-Acevedo NM, Ocampo AL, et al. Metal nanoparticle–carbon nanotubes hybrid catalysts immobilized in a polymeric membrane for the reduction of 4-nitrophenol. SN Applied Sciences. 2019;1(4).
[11] Ayodhya D, Perka S, Nambigari N. Sunlight-driven efficient photocatalytic and antimicrobial studies of microwave-assisted Ir-doped TiO2 nanoparticles for environmental safety. Nanochemistry Research. 2018;3(1):36-49.
[12] Wang S, Zhang J, Yuan P, Sun Q, Jia Y, Yan W, et al. Au nanoparticle decorated N-containing polymer spheres: additive-free synthesis and remarkable catalytic behavior for reduction of 4-nitrophenol. Journal of Materials Science. 2014;50(3):1323-32.
[13] Lv J-J, Wang A-J, Ma X, Xiang R-Y, Chen J-R, Feng J-J. One-pot synthesis of porous Pt–Au nanodendrites supported on reduced graphene oxide nanosheets toward catalytic reduction of 4-nitrophenol. Journal of Materials Chemistry A. 2015;3(1):290-6.
[14] Zhang P, Li R, Huang Y, Chen Q. A Novel Approach for the in Situ Synthesis of Pt–Pd Nanoalloys Supported on Fe3O4@C Core–Shell Nanoparticles with Enhanced Catalytic Activity for Reduction Reactions. ACS Applied Materials & Interfaces. 2014;6(4):2671-8.
[15] Sampurnama S, Muthamizha S, Dhanasekarana T, Lathaa Padmanabana A, Selvamb P, et al. Synthesis and characterization of Keggin-type polyoxometalate/zirconia nanocomposites—Comparison of its photocatalytic activity towards various organic pollutants. Journal of Photochemistry and Photobiology A: Chemistry. 2019;370:26-40.
[16] Ma J, Guo S, Guo X, Ge H. ZrO2@Ag composite catalyst for hydrogenation reduction of organic dye: Preparation and characterization as well as catalytic performance evaluation. Ceramics International. 2015;41(9):12453-8.
[17] Ayodhya D, Veerabhadram G. Microwave-assisted synthesis, characterization and photoluminescence interaction studies of undoped, Zr2+, Rh3+ and Pd2+ doped ZnS quantum dots. Materials Discovery. 2018;12:1-8.
[18] Ayodhya D, Veerabhadram G. Ternary semiconductor ZnxAg1−xS nanocomposites for efficient photocatalytic degradation of organophosphorus pesticides. Photochemical & Photobiological Sciences. 2018;17(10):1429-42.
[19] Gröttrup J, Paulowicz I, Schuchardt A, Kaidas V, Kaps S, Lupan O, et al. Three-dimensional flexible ceramics based on interconnected network of highly porous pure and metal alloyed ZnO tetrapods. Ceramics International. 2016;42(7):8664-76.
[20] Babu B, Mallikarjuna K, Reddy CV, Park J. Facile synthesis of Cu@TiO 2 core shell nanowires for efficient photocatalysis. Materials Letters. 2016;176:265-9.
[21] Ayodhya D, Veerabhadram G. One-pot green synthesis, characterization, photocatalytic, sensing and antimicrobial studies of Calotropis gigantea leaf extract capped CdS NPs. Materials Science and Engineering: B. 2017;225:33-44.
[22] Ayodhya D, Veerabhadram G. Green synthesis, characterization, photocatalytic, fluorescence and antimicrobial activities of Cochlospermum gossypium capped Ag2S nanoparticles. Journal of Photochemistry and Photobiology B: Biology. 2016;157:57-69.
[23] Ayodhya D, Veerabhadram G. Highly efficient sunlight-driven photocatalytic degradation of organic pollutants and fluorescence detection of Hg2+ using multifunctional GO-Bi2S3 nanostructures. Journal of Photochemistry and Photobiology A: Chemistry. 2018;356:545-55.
[24] Renuka L, Anantharaju KS, Sharma SC, Nagabhushana H, Vidya YS, Nagaswarupa HP, et al. A comparative study on the structural, optical, electrochemical and photocatalytic properties of ZrO2 nanooxide synthesized by different routes. Journal of Alloys and Compounds. 2017;695:382-95.
[25] Dwivedi R, Maurya A, Verma A, Prasad R, Bartwal KS. Microwave assisted sol–gel synthesis of tetragonal zirconia nanoparticles. Journal of Alloys and Compounds. 2011;509(24):6848-51.
[26] Vollath D, Sickafus KE. Synthesis of nanosized ceramic oxide powders by microwave plasma reactions. Nanostructured Materials. 1992;1(5):427-37.
[27] Lee WS, Kim SW, Koo BH, Bae DS. Synthesis and microstructure of Y2O3-doped ZrO2–CeO2 composite nanoparticles by hydrothermal process. Colloids and Surfaces A: Physicochemical and Engineering Aspects. 2008;313-314:100-4.
[28] Wu N-L, Wu T-F. Enhanced Phase Stability for Tetragonal Zirconia in Precipitation Synthesis. Journal of the American Ceramic Society. 2000;83(12):3225-7.
[29] Khan SA, Fu Z, Rehman SS, Asif M, Wang W, Wang H. Study of template-free synthesis hierarchical m-ZrO2 nanorods by hydrothermal method. Powder Technology. 2014;256:71-4.
[30] Tai CY, Hsiao B-Y. Characterization of zirconia powder synthesized via reverse microemulsion precipitation. Chemical Engineering Communications. 2005;192(11):1525-40.
[31] Razpotnik T, Maček J. Synthesis of nickel oxide/zirconia powders via a modified Pechini method. Journal of the European Ceramic Society. 2007;27(2-3):1405-10.
[32] Duran C, Sato K, Hotta Y, Göçmez H, Watari K. Ball milling assisted hydrothermal synthesis of ZrO2 nanopowders. Ceramics International. 2015;41(4):5588-93.
[33] Taguchi M, Nakane T, Matsushita A, Sakka Y, Uchikoshi T, Funazukuri T, et al. One-pot synthesis of monoclinic ZrO2 nanocrystals under subcritical hydrothermal conditions. The Journal of Supercritical Fluids. 2014;85:57-61.
[34] Angeles-Rosas M, Camacho-López MA, Ruiz-Trejo E. Structure, conductivity and luminescence of 8mol% scandia-doped zirconia prepared by sol–gel. Solid State

Ionics. 2010;181(29-30):1349-54.
[35] Gondal MA, Fasasi TA, Baig U, Mekki A. Effects of Oxidizing Media on the Composition, Morphology and Optical Properties of Colloidal Zirconium Oxide Nanoparticles Synthesized via Pulsed Laser Ablation in Liquid Technique. Journal of Nanoscience and Nanotechnology. 2018;18(6):4030-9.
[36] Smits K, Grigorjeva L, Millers D, Sarakovskis A, Grabis J, Lojkowski W. Intrinsic defect related luminescence in ZrO2. Journal of Luminescence. 2011;131(10):2058-62.
[37] Petrik NG, Taylor DP, Orlando TM. Laser-stimulated luminescence of yttria-stabilized cubic zirconia crystals. Journal of Applied Physics. 1999;85(9):6770-6.
[38] Reimann C, Bredow T. Adsorption of nitrogen and ammonia at zirconia surfaces. Journal of Molecular Structure: THEOCHEM. 2009;903(1-3):89-99.
[39] Liang J, Deng Z, Jiang X, Li F, Li Y. Photoluminescence of Tetragonal ZrO2Nanoparticles Synthesized by Microwave Irradiation. Inorganic Chemistry. 2002;41(14):3602-4.
[40] Tamrakar RK, Tiwari N, Dubey V, Upadhyay K. Infrared spectroscopy and luminescence spectra of Yb3+ doped ZrO2 nanophosphor. Journal of Radiation Research and Applied Sciences. 2015;8(3):399-403.
[41] File X-rPD. American Society for Testing Materials. Philadelphia, Pa. 1960:583.
[42] Jana S, Ghosh S, Nath S, Pande S, Praharaj S, Panigrahi S, et al. Synthesis of silver nanoshell-coated cationic polystyrene beads: A solid phase catalyst for the reduction of 4-nitrophenol. Applied Catalysis A: General. 2006;313(1):41-8.
[43] Song J-M, Zhang S-S, Yu S-H. Multifunctional Co0.85Se-Fe3O4Nanocomposites: Controlled Synthesis and Their Enhanced Performances for Efficient Hydrogenation ofp-Nitrophenol and Adsorbents. Small. 2013;10(4):717-24.
[44] Hayakawa K, Yoshimura T, Esumi K. Preparation of Gold–Dendrimer Nanocomposites by Laser Irradiation and Their Catalytic Reduction of 4-Nitrophenol. Langmuir. 2003;19(13):5517-21.
[45] Dong K, Liu Z, Ren J. A general and eco-friendly self-etching route to prepare highly active and stable Au@metal silicate yolk-shell nanoreactors for catalytic reduction of 4-nitrophenol. CrystEngComm. 2013;15(32):6329.